Table 1
The estimated number of injected cells labeled by QDs contained in each organ at indicated days after injection

Time	Organ	QD-labeled cells in each section (cells/section)	Estimated cell numbers in each organ ($\times 10^4$ cells/organ)
2 h	Spleen	605 ± 133	41.2 ± 13.4 (4.1%)
	Kidney	Not detected	Not detected
	Liver	1.0 ± 1.0	0.58 ± 0.63 (0.06%)
	Lung	46.7 ± 18.0	18.6 ± 71.9 (1.86%)
3 days	Spleen	97.7 ± 27.7	6.64 ± 2.44 (0.66%)
	Kidney	0.33 ± 0.58	0.04 ± 0.07 (0.004%)
	Liver	2.0 ± 1.0	1.16 ± 0.68 (0.12%)
	Lung	47.3 ± 5.0	18.5 ± 2.15 (1.85%)
7 days	Spleen	72.0 ± 10.8	4.90 ± 1.24 (4.9%)
	Kidney	1.3 ± 0.6	0.15 ± 0.09 (0.15%)
	Liver	10.6 ± 2.1	6.17 ± 1.75 (6.1%)
	Lung	51.6 ± 11.0	20.1 ± 4.52 (20.1%)

QD-labeled cells including each organ section were counted ($n = 3$). The estimated cell numbers in each organ were the presumed value calculated from the volume of the organs and the number of QD-labeled cells contained in the sections. The data are presented as means ± standard deviation. The value in parentheses shows the percentages of the injected QD-labeled cells located in each organ.

became lower after more than 24 h culture. Moreover, QDs held in endosomes were gradually concentrated in a time-dependent manner. The distribution of QDs may incline toward the specific position in a cell, which resulted in that QD may be unevenly distributed to the two product cells at cell division. Probably QDs may be eliminated from injected cells in the same way in vivo. Furthermore, the influence by cell division in the mouse cannot be disregarded either. As shown in Fig. 6, injected EL-4 cells were grown after 5 days (*right graphs*) and detection of QD-labeled cells became difficult 5 days after injection (*left graphs*). Thus, cell labeling using QDs may tend to be influenced by cell division. The second possibility was exclusion of injected cells by the host–immune system. QDs holding cells may be vanishing more rapidly out of the blood circulation by some active pathways in the early stage after injection. As we surmised that QDs were excluded by the spleen function, QD-labeled cells were detected from the sections of the kidneys, liver, lung, and spleen. Approximately 20% of injected QD-labeled cells were accumulated in those four organs up to 7 days after injection. The last possibility was the loss of photoluminescent ability of the QDs. It was known that the fluorescence emitted from QDs was attenuated by depriving of electric charge on QDs. We assumed that the degradation of the surface of QDs in endosomes including QDs was due to a change of the pH as a consequence of activation of T cells. But as shown in Fig. 4, no significant fluorescent elimination was observed although QD-holding lymphocytes were stimulated with calcium ionophore A23187, PMA, and some lectins such as ConA and PHA.

Our approaches suggest that QDs can be traced using the injected cells for more than a week by quite easy techniques. In this approach, QDs had many more advantageous points than organic fluorophores. As shown in Fig. 5, the fluorescent intensity of QDs was approximately equal to that of the organic fluorophores in short-time exposure such as flow cytometry, but the fluorescence of QDs was superior to that of organic fluorophores in terms of the operating lifetime. QDs could be applied not only to cell labeling marker but also to real-time single-molecule bioimaging for several minutes in living cells, such as antigen–antibody reactions, the moment of viral infection, the movement of transcription in nuclei, and more. More improvements may be achieved by multicolor scanning using some QDs of different particle sizes [22].

At present, no damage or toxicity caused by injection of QD-labeled cells over individuals was observed although the adverse effects on the organisms by the QDs were anticipated, and cytotoxicity was observed at high concentration of QDs. Efforts to address this issue are being made in developing a different silicon based QD. Further miniaturization of the particle is anticipated and silicon-based QDs are expected to be much safer because neither cadmium nor selenium is used. Advanced surface treatment and improved introducing-methods of QDs were required to retain the QDs inside the cells for a longer and more stable duration. Nowadays, another introduction method that encapsulated individual nanocrystals in liposomes is being considered [23–25]. QDs could be used in both carrier or drug delivery systems and to assess the effects of treatment by combining this method and the other gene targeting therapy using the liposomes if a semi-permanent cell labeling technique was enabled in those methods [26]. Furthermore, a small tumor can be detected by specific wavelength infrared rays emitted from some QDs, as the QDs can be conjugated with biomolecules which can specifically recognize tumor cells in a similar way as antibodies and some lectins [27]. Visualization of QDs which flowed in the blood of the capillary vessels and which were accumulated in adipose tissue has already been reported using multiphoton microscopy [28].

The dynamics of QDs in this application is dependent on the albumin conjugating on the surface of the QDs. Further, it may be expected to conjugate QDs with various proteins or molecules for the carrier molecules of drug delivery system or cell specific marker. With the development of new surface treatments of QDs, it may soon become possible to make these possibilities come true using various methods to replace the conventional organic fluorophores that are currently being used.

Acknowledgments

We are grateful to Drs. Tomokazu Nagao, Ken Murayama, and Wayne Dawson (National Institute of Infectious Diseases) for valuable advice and help with data collection, animal treatment, and proofreading. This work was supported by Grant 'H14-nano-004' of the Ministry of Health, Labor and Welfare of Japan.

References

[1] S.J. Rosenthal, I. Tomlinson, E.M. Adkins, S. Schroeter, S. Adams, L. Swafford, J. McBride, Y. Wang, L.J. DeFelice, R.D. Blakely, Targeting cell surface receptors with ligand-conjugated nanocrystals, J. Am. Chem. Soc. 124 (2002) 4586–4594.

[2] B. Dubertret, P. Skourides, D.J. Norris, V. Noireaux, A.H. Brivanlou, A. Libchaber, In vivo imaging of quantum dots encapsulated in phospholipid micelles, Science 298 (2002) 1759–1762.

[3] G.T. Shubeita, S.K. Sekatskii, G. Dietler, I. Potapova, A. Mews, T. Basch, Scanning near-field optical microscopy using semiconductor nanocrystals as a local fluorescence and fluorescence resonance energy transfer source, J. Microsc. 210 (2003) 274–278.

[4] H. Xu, M.Y. Sha, E.Y. Wong, J. Uphoff, Y. Xu, J.A. Treadway, A. Truong, E. O'Brien, S. Asquith, M. Stubbins, N.K. Spurr, E.H. Lai, W. Mahoney, Multiplexed SNP genotyping using the Qbead system: a quantum dot-encoded microsphere-based assay, Nucleic Acids Res. 31 (2003) 43.

[5] X. Wu, H. Liu, J. Liu, K.N. Haley, J.A. Treadway, J.P. Larson, N. Ge, F. Peale, M.P. Bruchez, Immunofluorescent labeling of cancer marker Her2 and other cellular targets with semiconductor quantum dots, Nat. Biotech. 21 (2003) 41–46.

[6] W.C. Chan, D.J. Maxwell, X. Gao, R.E. Bailey, M. Han, S. Nie, Luminescent quantum dots for multiplexed biological detection and imaging, Curr. Opin. Biotech. 13 (2002) 40–46.

[7] H. Mattoussi, J.M. Mauro, E.R. Goldman, G.P. Anderson, V.C. Sundar, F.V. Mikulec, M.G. Bawendi, Self-assembly of CdSe–ZnS quantum dot bioconjugates using an engineered recombinant protein, J. Am. Chem. Soc. 122 (2000) 12142–12150.

[8] S.A. Weston, C.R. Parish, New fluorescent dyes for lymphocyte migration studies. Analysis by flow cytometry and fluorescence microscopy, J. Immunol. Methods 133 (1990) 87–97.

[9] A.B. Lyons, C.R. Parish, Determination of lymphocyte division by flow cytometry, J. Immunol. Methods 171 (1994) 131–137.

[10] M. Bruchez Jr., M. Moronne, P. Gin, S. Weiss, A.P. Alivisatos, Semiconductor nanocrystals as fluorescent biological labels, Science 281 (1998) 2013–2016.

[11] W.C. Chan, S. Nie, Quantum dot bioconjugates for ultrasensitive nonisotopic detection, Science 281 (1998) 2016–2018.

[12] X. Gao, W.C. Chan, S. Nie, Quantum-dot nanocrystals for ultrasensitive biological labeling and multicolor optical encoding, J. Biomed. Opt. 7 (2002) 532–537.

[13] E.R. Goldman, E.D. Balighian, H. Mattoussi, M.K. Kuno, J.M. Mauro, P.T. Tran, G.P. Anderson, Avidin: a natural bridge for quantum dot-antibody conjugates, J. Am. Chem. Soc. 124 (2002) 6378–6382.

[14] D. Gerison, F. Pinaud, S.C. Williams, W.J. Parak, D. Zanchet, S. Weiss, A.P. Alivisatos, Synthesis and properties of biocompatible water-soluble silica-coated CdSe/ZnS semiconductor quantum dots, J. Phys. Chem. 105 (2001) 8861–8871.

[15] I.L. Medintz, A.R. Clapp, H. Mattoussi, E.R. Goldman, B. Fisher, J.M. Mauro, Self-assembled nanoscale biosensors based on quantum dot FRET donors, Nat. Mater. 9 (2003) 630–638.

[16] E.R. Goldman, G.P. Anderson, P.T. Tran, H. Mattoussi, P.T. Charles, J.M. Mauro, Conjugation of luminescent quantum dots with antibodies using an engineered adaptor protein to provide new reagents for fluoroimmunoassays, Anal. Chem. 74 (2002) 841–847.

[17] K. Hanaki, A. Momo, T. Oku, A. Komoto, S. Maenosono, Y. Yamaguchi, K. Yamamoto, Semiconductor quantum dot/albumin complex is a long-life and highly photostable endosome marker, Biochem. Biophys. Res. Commun. 302 (2003) 496–501.

[18] J.K. Jaiswal, H. Mattoussi, J.M. Mauro, S.M. Simon, Long-term multiple color imaging of live cells using quantum dot bioconjugates, Nat. Biotech. 21 (2003) 47–51.

[19] H. van Dekken, A. Hagenbeek, J.G. Bauman, Detection of host cells following sex-mismatched bone marrow transplantation by fluorescent in situ hybridization with a Y-chromosome specific probe, Leukemia 10 (1989) 724–728.

[20] R. Rizzuto, M. Brini, P. Pizzo, M. Murgia, T. Pozzan, Chimeric green fluorescent protein as a tool for visualizing subcellular organelles in living cells, Curr. Biol. 5 (1995) 635–642.

[21] C. Kaether, H.H. Gerdes, Visualization of protein transport along the secretory pathway using green fluorescent protein, FEBS Lett. 369 (1995) 267–271.

[22] Y.T. Lim, S. Kim, A. Nakayama, N.E. Stott, M.G. Bawendi, J.V. Frangioni, Selection of quantum dot wavelengths for biomedical assays and imaging, Mol. Imaging 2 (2003) 50–64.

[23] A. Hayashi, T. Nakanishi, J. Kunisawa, M. Kondoh, S. Imazu, Y. Tsutsumi, K. Tanaka, H. Fujiwara, T. Hamaoka, T. Mayumi, A novel vaccine delivery system using immunopotentiating fusogenic liposomes, Biochem. Biophys. Res. Commun. 261 (1999) 824–828.

[24] T. Nakanishi, A. Hayashi, J. Kunisawa, Y. Tsutsumi, K. Tanaka, Y. Yashiro-Ohtani, M. Nakanishi, H. Fujiwara, T. Hamaoka, T. Mayumi, Fusogenic liposomes efficiently deliver exogenous antigen through the cytoplasm into the MHC class I processing pathway, Eur. J. Immunol. 30 (2000) 1740–1747.

[25] J. Kunisawa, T. Nakanishi, I. Takahashi, A. Okudaira, Y. Tsutsumi, K. Katayama, S. Nakagawa, H. Kiyono, T. Mayumi, Sendai virus fusion protein mediates simultaneous induction of MHC class I/II-dependent mucosal and systemic immune responses via the nasopharyngeal-associated lymphoreticular tissue immune system, J. Immunol. 167 (2001) 1406–1412.

[26] M. Harada-Shiba, K. Yamauchi, A. Harada, I. Takamisawa, K. Shimokado, K. Kataoka, Polyion complex micelles as vectors in gene therapy–pharmacokinetics and in vivo gene transfer, Gene Ther. 9 (2002) 407–414.

[27] M.E. Akerman, W.C. Chan, P. Laakkonen, S.N. Bhatia, E. Ruoslahti, Nanocrystal targeting in vivo, Proc. Natl. Acad. Sci. USA 99 (2002) 12617–12621.

[28] D.R. Larson, W.R. Zipfel, R.M. Williams, S.W. Clark, M.P. Bruchez, F.W. Wise, W.W. Webb, Water-soluble quantum dots for multiphoton fluorescence imaging in vivo, Science 300 (2003) 1434–1436.

特集にあたって

A new technology developing diagnoses and evaluation of therapy by bioimaging——Introduction

鈴木和男
Kazuo Suzuki
国立感染症研究所生物活性物質部，日本バイオイメージング学会会長

治療や医薬の安全性が重視されている今日，安全で経済性の高い医薬の提供，非侵襲性の診断法や治療判定，医薬・診断の安全性の評価など，これまでにない医療分野での新しい技術の開発が要望されている．一方，治療薬の開発には莫大な費用がかかり，ひいては薬価へそれがはねかえってくる．また，臨床試験にも莫大な費用と時間がかかり，審査基準も厳しい状況から，多くの日本の製薬企業は海外で臨床試験，審査をしているともいわれている．このような現状のなかにあって，あらたな診断法，治療評価法を開発し，的確で簡便な方法を利用した日本発信のテクノロジーを使った医療分野の発展を考えなくてはならない時代にさしかかっている．

このような状況のなか，昨年(2003)から今年(2004)はじめにかけて“バイオイメージングによる医療応用をめざした”シンポジウムを3回企画した[1-3]．このときのテーマをもとに，医療応用に関連するバイオイメージングの研究者に，今回の特集のメインテーマ“バイオイメージングが切り開くあらたな診断・治療評価技術”に沿って執筆してもらうことにした．

これからの新しい“診断法”や“治療評価”に，“ナノテクノロジー”で開発された微小な分子や，微細な構造解析法も使ってバイオイメージングのテクノロジーを利用することが日常的になってきている．つまりイメージング技術とナノテクノロジーとの融合による医学・生物の現象解析が不可欠になりつつあることを物語っている．その意味で，バイオイメージング技術は医療の先端技術であり，その医用応用への研究が急速に進展しつつある．このように，バイオイメージングの技術は医療分野での応用に取り入れられる状況になっている．その背景には医学・生物学において“みる技術”を活用した“バイオイメージング”が定着していることがあげられる．

そこで今回は，新しいテクノロジーの創出による治療法・診断の方法の基礎や新しい治療法の開発などに主眼をおいた特集を企画した．

文献

1) 日本バイオイメージング学会・他：シンポジウム，バイオイメージングとナノテクノロジー．東京，2003年2月20〜21日．
2) 日本バイオイメージング学会・他：シンポジウム，ナノとバイオの融合学理構築，産業基盤形成．松島，2003年9月10〜11日．
3) 日本バイオイメージング学会・他：シンポジウム，バイオイメージング—最近の進歩と医療への応用．東京，2004年1月9日．

血管炎初期反応のイメージング

In vivo imaging of MPO-ANCA related glomerulonephritis in mouse

長尾朋和(写真)　鈴木和男
Tomokazu Nagao and Kazuo Suzuki
国立感染症研究所生物活性物質部

◎腎炎，SLE，リウマチをはじめとする難治性血管炎は，自己免疫疾患などの免疫異常による好中球の活性化や好中球自己抗体と連動して進行するものと予想されている．著者らはそのなかでもANCA陽性の急速進行性糸球体腎炎に注目し，その炎症初期に起こるであろうと考えられる血管傷害について，腎血流の *in vivo* イメージング手法を用いて検討した．本稿ではその手法と結果について，概略を解説したい．

Key word：好中球自己抗体，糸球体腎炎，*in vivo* イメージング

MPO-ANCA陽性糸球体腎炎

Anti-neutrophil cytoplasmic antibody(ANCA)陽性の急速進行性糸球体腎炎は，わが国においてはmyeloperoxidase(MPO)を抗原とするMPO-ANCAの抗体価が上昇するタイプが多くみられる[1]．MPO-ANCA陽性の半月体形成性腎炎は糸球体基底膜に補体や免疫グロブリンの沈着を認めないpauci-immune型であることが特徴であるが，現在のところ，このような特徴を示し，かつMPO-ANCA単独で半月体形成性腎炎を誘導できる動物モデルはXiaoらの報告[2]を除いて存在しない．MPOがMPO-ANCAの抗原になっていることはMPO欠損マウスで明らかにされており[3]，ほかにもリスクファクターとなるようなサイトカインやケモカインが報告されている[4,5]が，これらとMPO-ANCAがどのように血管炎の発症・進展にかかわっているのか，いまだ明らかになっていないのが現状である．また，上記のように最適な動物モデルが存在しないため，これまでMPO-ANCAに関して得られた知見の多くは *in vitro* における実験によるものであった．しかし，今後のより詳細な発症メカニズムの検討や，グロブリン治療[6]などの治療効果を含めた解析を行ううえでは，*in vivo* における解析手法の確立が重要視されてきている．

腎微小血管傷害を起こす誘導型モデルマウス

著者らも，MPO-ANCAとしてpolyclonal rabbit anti-mouse MPO antibody(anti-mMPO)のみをC57BL/6マウスに静脈内投与した場合，anti-mMPOのみではマウスに腎炎を発症させることが不可能であった．そこで，モデルには *Candida albicans* 由来糖ペプチドCAWS，polyclonal rabbit anti-mouse MPO antibody(anti-mMPO)およびfMet-Leu-Phe(FMLP)の3種類の物質を組み合わせて用いた．CAWSは大野らによって作製されたもので，比較的大きいサイズの動脈に血管炎を誘導することが知られている[7,8]．また，FMLPは好中球走化性因子であり，これを用いて好中球を活性化することができる．そこで，これらを静脈内投与することで，急性的に腎微小血管傷害を起こす誘導型モデルマウスの確立をめざした．最終的なプロトコールはC57BL/6マウス(雄，9週齢)にCAWS(150 μg/mouse)を静脈内投与し，その3

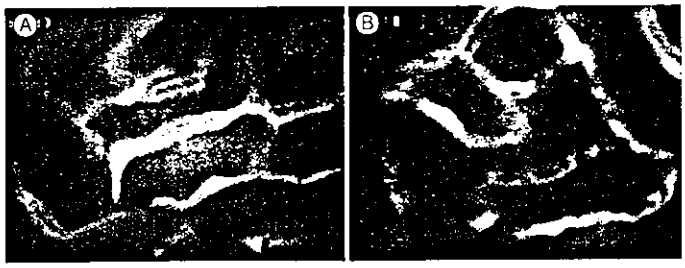

図1　コントロールマウス(A)およびCAWS+anti-mMPO+FMLPを投与したマウス(B)の腎表面血流
FITC-dextranによって蛍光を発し，白くみえる網目状の部分が毛細血管で，血管以外の暗い部分は尿細管である．コントロールマウスでは血流速度が速いため，個々の血球細胞を確認することができないが，腎炎を誘導したマウスでは血流が停止しつつあるため，赤血球などが黒いスポットとして確認できる．

時間後にanti-mMPO(1 mg/mouse)を，加えて5日後にfMet-Leu-Phe(FMLP，10^{-8}mol/mouse)を静脈内投与するものである．このモデルマウスは慢性的な腎炎を引き起こすものではないが，FMLPの投与から一過性の蛋白尿などの特徴を示し，さらに糸球体には微小血栓もみられるなど，糸球体毛細血管に何らかの傷害を与えるものであった．

In vivo イメージング

著者らはこのモデルマウスの評価手段として，*in vivo* イメージングを利用した．とくに血管炎のように血管がおもな傷害の場となる場合，血流のような生体内のダイナミックな変化をとらえることが可能な*in vivo* イメージング技術は非常に有用である．また，組織学的には変化が確認できないような，炎症における比較的初期段階を評価するためにも最適な手法といえる．これまでにも透過光による観察が容易な腸間膜微小循環系を対象とした研究が行われてきたが，実質臓器レベルにおいても臓器自体の厚みのために光透過が非常に悪いものの，蛍光物質をトレーサーとした臓器表層の血流観察が可能であり，これによって多くのあらたな知見が報告されてきている．著者らが観察対象とした腎は臓器全体に毛細血管がはりめぐらされており，血液による光吸収の影響が大きいため，糸球体毛細血管の血流状態を観察することは非常に困難であった．しかし，リアルタイム共焦点顕微鏡[9]や2光子励起顕微鏡[10]などを用いて糸球体血流を可視化することが可能になってきている．

著者らの用いた実験系は通常の蛍光顕微鏡観察と同様で非常にシンプルであり，モデルマウスの血流は蛍光物質FITC-dextranを用いて可視化することとした．FITC-dextranの分子量は約280,000であり，通常の機能を有した血管であれば，血管外に漏れ出すことはない．すなわち，蛍光顕微鏡観察を行ったときに血漿のみが蛍光を発することとなる．また，特殊な細胞以外にはほとんど取り込まれないため，赤血球などは蛍光を発しない．実際の手順としては，麻酔下のマウスにFITC-dextranを尾静脈投与した後，背部を切開し腎のみを露出させた後，これを生存状態のまま倒立顕微鏡下において蛍光観察した．また，観察中はヒーティングプレートを用いて37℃に保ち，さらに生理食塩水を用いて臓器の乾燥を防いだ．この方法によって腎表面を流れる尿細管周囲毛細血管の可視化が可能となり，また腎表面より50 μm以内に存在する糸球体であれば，その毛細血管を可視化することも可能となった．しかし，残念ながら腎表面より50 μm以内に存在する糸球体は非常に少なく，その後の解析に供する量の映像は得られなかった．そこで，観察対象となる血管は尿細管周囲毛細血管とし，その血流動態をDVDレコーダーで録画した後，画像解析を行った．

モデルマウスにおける血流の悪化

この観察手法を用いて確立した誘導型モデルマ

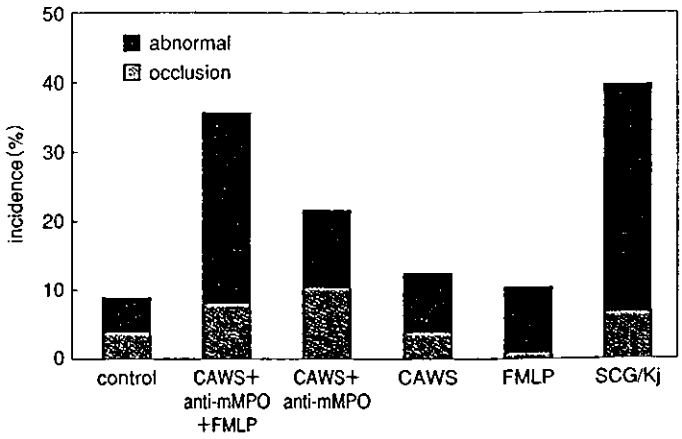

図 2　各投与条件における血流が停止した血管(occulusion)と異常な血流がみられる血管(abnormal)の割合

CAWS, FMLP, anti-mMPO の 3 種類すべてを投与した場合において顕著な血流停止，異常血流が観察され，糸球体腎炎の自然発症マウスである SCG/Kj マウスにおいても同程度の血流停止や異常血流がみられた．

ウスおよび無処理のコントロールマウスにおける腎血流動態を比較したところ，モデルマウスにおいて顕著な腎微小循環の悪化が観察された(図 1)．具体的には血流速度の低下・血流停止・血液の逆流などの現象が観察され，CAWS または FMLP 単独投与の場合と比較し，anti-mMPO を投与した場合に血流停止(occlusion)が誘発され(観察した血管の約 10%)，さらに 3 種類すべてを投与した場合には広範囲にわたる腎表面血流の悪化(abnormal)が観察された(観察した血管の約 30%)(図 2)．このような腎表面血流の悪化は，糸球体腎炎の自然発症マウスである SCG/Kj マウスにおいても同様にみられた．さらに，この腎微小循環の悪化には血管内皮への白血球の接着を伴ったものもみられ，anti-mMPO を用いたこの腎炎誘導モデルにおいては MPO の関与が予想されることから，観察された白血球のなかでもとくに MPO を発現している好中球が炎症における重要な役割を担っているものと考えられる．

おわりに

血管炎初期反応のイメージングとして，とくに糸球体腎炎を対象とした *in vivo* イメージングを紹介した．本手法により血管内で起こっている現象をリアルタイムにとらえることが可能となり，その結果，MPO-ANCA が関連する血管炎の初期において，内皮細胞への白血球の接着とそれによる血流の悪化がみられることが明らかとなった．近年のコンピュータ画像処理技術の進歩によって顕微鏡の性能も向上してきており，上記の高速共焦点顕微鏡や 2 光子励起顕微鏡など，*in vivo* イメージングにより適した顕微鏡も開発されてきている．今後，これらの顕微鏡技術を用いた新しい知見が期待される．

なお，本研究は厚生労働科研費により行われた．

文献

1) 中林公正，土岐岳士：ANCA 関連血管炎の臨床像．医学のあゆみ，**206**：130-132，2003.
2) Xiao, H. et al.：Antineutrophil cytoplasmic autoantibodies specific for myeloperoxidase cause glomerulonephritis and vasculitis in mice. *J. Clin. Invest.*, **110**：955-963, 2002.
3) Ishida-Okawara, A. et al.：Contribution of myeloperoxidase to coronary artery vasculitis associated with MPO-ANCA production. *Inflammation*, **25**：381-387, 2001.
4) Cockwell, P. et al.：Interleukin-8：A pathogenic role in antineutrophil cytoplasmic autoantibody-associated glomerulonephritis. *Kidney Int.*, **55**：852-863, 1999.
5) Arimura, Y. et al.：Serum myeloperoxidase and serum cytokines in anti-myeloperoxidase antibody-associated glomerulonephritis. *Clin. Nephrol.*, **40**：

256-264, 1993.
6) Jayne, D. R. W. et al. : Intravenous immunoglobulin for ANCA-associated systemic vasculitis with persistent disease activity. *Q. J. Med.*, **93** : 433-439, 2000.
7) 大野尚仁：血管炎を誘導する真菌糖蛋白質の免疫活性化. 医学のあゆみ, **206** : 150-152, 2003.
8) Ohno, N. : Chemistry and biology of angiitis inducer, *Candida albicans* water-soluble mannoprotein-β-glucan complex(CAWS). *Microbiol. Immunol.*, **47** : 479-490, 2003.
9) Oyanagi-Tanaka, Y. et al. : Real-time observation of hemodynamic changes in glomerular aneurysms induced by anti-Thy-1 antibody. *Kidney Int.*, **59** : 252-259, 2001.
10) Dunn, K. W. et al. : Functional studies of the kidney of living animals using multicolor two-photon microscopy. *Am. J. Physiol. Cell Physiol.*, **283** : C905-C916, 2002.

腎臓血管傷害のイメージング

国立感染症研究所生物活性物質部*，東京理科大学理工学部** 長尾 朋和*，村山 研*·**，越尾 修*
東京薬科大学薬学部#，東邦大学医学部大橋病院## 大野 尚仁#，三浦 典子#，高橋 啓##
オタゴ大学(ニュージーランド)' 馬渕 綾子'，南谷 晴之''
慶應義塾大学大学院基礎理工学部'' 鈴木 和男*·**

要 旨

腎炎，動脈炎，SLEなどの難治性血管炎は，好中球自己抗体(anti-neutrophil cytoplasmic antibodies；ANCA)が血清中に検出される自己免疫疾患で，免疫異常や好中球活性化と連動して進行するものと予想されている。好中球活性化の関与については，病理組織切片の観察の知見によっているが，生体ではどのような状況で活性化されているかは明らかではない。おそらく，*in vivo*での血管内部は，血管炎に伴って，血圧・血流速度などの血行力学的因子が変化していると想像される。これらの血流因子の変化を*in vivo*で解析し，血管傷害の要因を検証することが必要である。この方法には，顕微鏡を用いた*in vivo*の生存状態で，臓器微小循環血流を観察して，血流のパラメーターを定量的に評価することが必要である。この方法により，腎炎において重要な働きを担っているものと思われる好中球の動態も*in vivo*での観察・解析が可能である。そこでわれわれは，腎炎の発症・進展におけるANCAおよび好中球の役割を明らかにするために，腎炎モデルマウスの構築およびin vivoイメージング観察を行った。その結果，*Candida albicans*由来糖ペプチド(CAWS)，rabbit anti-mouse myeloperoxidase(anti-mMPO)およびfMet-Leu-Pheによって腎血管傷害を誘導したC57BL/6マウスでは，血流速度の低下，血流停止，血液の逆流などが観察され，最も顕著な場合，広範囲にわたる腎表面血流の停止も観察された。さらに，これらの現象には血管内皮への白血球の接着も観察された。本腎炎誘導モデルにおいては，myeloperoxidase(MPO)が関連していることから，観察された白血球のなかでも特に好中球が炎症における重要な役割を担っているものと考えられる。本血管炎誘導モデルにおいて開発したin vivoイメージングの評価法は，血管炎の進行によって誘発される多臓器不全の治療法の開発や，治癒機転および発症機構を解析するうえで有用であることを示した。

I．緒 言

難治性血管炎は，腎炎，動脈炎やSLEなどとして顕れ，その要因の1つにANCAが，血清中に増加することが明らかにされてきている[1-4]。このように，難治性血管炎には，自己免疫疾患などの免疫異常が関与している[5]。また，ANCAの対応分子の主なものが，好中球顆粒酵素のprotease-3(PR-3)やMPOであることから，好中球の活性化が発症や病態に関与していることが予想される[6,7]。

また，生体防御機能の不全は，好中球や免疫細胞の機能破綻やそれによるサイトカインの異常なネットワークのかく乱を誘導し，種々の臓器障害をもたらす。血管内皮細胞は，サイトカインと活性化白血球の攻撃にさらされ，また，臓器内での異常反応の前線となる。特に，好中球活性化は，難治性血管炎の発症およびその要因になっていることが強く示唆されており，好中球の殺菌酵素であるMPOがMPO-ANCAの抗原になっていることをわれわれは明らかにした[8]。すなわち，ANCAが好中球を活性化し，血管炎の発症に関わっている可能性を示唆した[9,10]。

一方，血管炎の病初期には，病理組織切片の観察から好中球が浸潤していることから裏付けられている。しかし，病理所見による*in vitro*の観察は，生体の生きたままでの観察ではないことから，生体での状況をそのまま解析することはできない。血管炎に伴って，生体の血管内部では，血圧・血

流速度などの血行力学的因子が変化していると推定されるが，*in vitro*では，これらの因子の変化をとらえることはかなり困難である。しかしながら，これらの因子が血管傷害に影響を及ぼすかを検証することが必要である。そこで，顕微鏡を用いた*in vivo*の観察システムより，生存状態で臓器微小循環血流を観察して，これらのパラメーターを定量的に評価することが必要である。さらに，重要な働きを担っているものと推定されている好中球の血管内部での動態も，本システムを使って*in vivo*での観察・解析をすることも重要である。一方，本システムの開発には，動物モデルが必要である。そこで，カンジダ菌成分Candida albicans derived substances (CADS)の接種による好中球抗体MPO-ANCAが血中に増加する冠状動脈炎モデルを用いた[11]。また，カンジダ菌外成分CAWSも血管炎を強く誘導することが可能である。

そこで，本研究では，CAWSによる腎傷害モデルマウスを作製し，本モデルマウスにより，in vivoイメージング法を開発した。それにより，腎炎の発症・進展におけるANCAおよび好中球の役割を検討した。

Ⅱ．研究方法

①多臓器不全関連血管炎モデルマウスの調整：*C. albicans*由来物質CAWSを投与して誘導した。

②in vivo イメージング：C57BL/6マウス(オス，9週齢)にCAWS(150 mg/mouse)をiv投与し，3時間後にanti-mMPO(rabbit anti-mouse myeloperoxidase，1 mg/mouse)をiv投与した。5日後，同様にCAWSとanti-mMPOを投与した後，fMet-Leu-Phe(FMLP，10^{-8} mol/mouse，細菌由来トリペプチド)をiv投与し，その3日後に腎表面における血流状態を観察した。血流の可視化にはFITC-dextranを用い，各マウスの腎表面における尿細管周囲毛細血管の血流を観察した。観察される血流動態は顕微鏡に接続したビデオカメラで撮影し，DVDに録画した。

Ⅲ．結　果

腎血管傷害を誘導するためにCAWS，anti-mMPOおよびfMet-Leu-Pheを投与し，腎臓表面血管のin vivoイメージングにより，血流速度の低下，血流停止，血液の逆流を観察・解析した。

①PBS投与のコントロールマウスでの腎臓血管の血流を観察した(図1)。

図1．コントロールマウスの腎血管のin vivoイメージング

②CAWS，anti-mouseMPOおよびfMet-Leu-Pheの投与による腎微小循環傷害のin vivoイメージング。

CAWS，anti-mouseMPOおよびfMet-Leu-Pheの投与によって，腎微小循環が悪化する様子がin vivoイメージングにより観察された(図2)。CAWSの投与によって，冠状動脈炎が誘導された。その頻度は，100%近い値を示した。この濃度以上の投与は，全身性の多臓器不全様ショックにて死亡した。また，in vivoイメージングの解析では，血流速度の低下，血流停止，血液の逆流が観察され，腎表面血流の停止がみられた(図2)。

③血流遮断と血管内皮細胞への白血球接着。

腎臓表面血管の流速の変化も，CAWS＋anti-mouseMPO＋fMet-Leu-Pheのときに悪化した。血流速度の低下・血流停止・血液の逆流などの現象が観察され，CAWSまたはFMLP単独投与の場合と比較し，両者に加えてanti-mMPOを投与した場合に血流停止が誘発され(観察した血管の約10%)，広範囲にわたる腎表面血流の悪化が観察された(約30%)。さらに，この腎微小循環の悪化には血管内皮細胞への白血球の接着を伴ったものもみられた(図3)。

C57BL/6マウスにCAWS，anti-mMPOおよびfMet-Leu-Pheを投与して誘導される腎血管傷害をin vivoイメージングにより，血流速度の低下，血流停止，血液の逆流を観察した。また，広範囲にわたる腎表面血流の停止も観察した。さらに，これらの現象には血管内皮への白血球の接着を伴ったものも観察された。

Ⅳ．考　察

CAWSによって，冠状動脈炎が100%近く発症し，投与量の増加により，多臓器不全様ショックで死亡した。この血管炎誘導モデルにおいては，*C. albicans*由来糖ペプチドCAWSが，MPOおよびMPO-ANCA産生と発症誘導に不可欠であることから，CAWSなどの真菌由来分子がサイトカインと連動して好中球を活性化して，多臓器不全様の症状を誘発する役割を担っているものと考えられる。その結果，急速な血管炎を誘発し，ひいては，多臓器不全をきたしたと考えられる。そのCAWSに加え，anti-mouseMPOおよびfMet-Leu-Pheを投与し，in vivoイメージングすることにより，血流速度の低下，血流停止，血液の逆流が観察され，腎表面血流の停止や血管内皮への白血球の接着も

図2．CAWS誘導の腎血管傷害in vivoイメージング
CAWS＋anti-mMPO＋FMLP

図3．CAWS誘導の腎血管傷害in vivoイメージングにおける血管内皮への白血球の接着

みられた。この*in vivo*での現象が，腎血管傷害の誘導を説明できると思われるが，分子機構との関係を明らかにする必要があり，さらに検討する必要がある。CAWSおよびanti-mMPOによって誘導される腎微小血管傷害誘導モデルを用いたin vivoイメージングの解析から以下のような推論が得られた。まずCAWSによって好中球数の増加・好中球活性化が誘発される。この状態において投与された好中球自己抗体(anti-mMPO)は，活性化によって細胞膜表面へ移行したMPOと複合体を形成し，さらなる好中球の活性化・血管内皮細胞への接着・活性酸素種の産生を引き起こすと考えられる。このことから，白血球のなかでも特に好中球が炎症における重要な役割を担っているものと推察される。また，このin vivoイメージング解析による評価法は，CAWS誘導血管炎やSCG/Kjマウスなどの腎炎モデル[12)-14)]での発症機構の解析に有用であり，本システムの利用が期待される。また，血管炎の治療法[15)-17)]の新しい評価系として有用であると思われる。このように，微小血管傷害を生体内で観察するシステムは，血管炎や多臓器不全の治療法の評価や治癒機構の解析として，今後の利用が期待される。

文　献

1) Jennette JC, Falk RJ：Antineutrophil cytoplasmic autoantibodies and associated diseases：a review. Am J Kidney Dis 15：517－529, 1990
2) Suzuki K：Neutrophil functions of patients with vasculitis related to MPO-ANCA. Int J Hematol 74：134－143, 2001
3) Savage COS, Winearls CG, Jones SJ, et al：Prospective study of radioimmunoassay for antibodies against neutrophil cytoplasm in diagnosis of systemic vasculitis. Lancet 1：1389－1393, 1987
4) Cohen Tervaert JW, Goldschmeding R, Elema JD, et al：Autoantibodies against myeloid lysosomal enzymes in crescentic glomerulonephritis. Kidney Int 37：799－806, 1990
5) Harper JM, Thiru S, Lockwood CM, et al：Myeloperoxidase autoantibodies distinguish vasculitis mediated by anti-neutrophil cytoplasm antibodies from immune complex disease in MRL/Mp-lpr/lpr mice：a spontaneous model for human microscopic angitis. Eur J Immunol 28：2217－2226, 1998
6) Tomizawa K, Mine E, Fujii A, et al：A panel set for epitope analysis of myeloperoxidase (MPO)-specific antineutrophil cytoplasmic antibody MPO-ANCA using recombinant hexamer histidine-tagged MPO deletion mutants. J Clin Immunol 18：142－152, 1998
7) Fujii A, Tomizawa K, Arimura Y, et al：Epitope analysis of myeloperoxidase (MPO) specific anti-

neutrophil Cytoplasmic autoantibodies (ANCA) in MPO-ANCA-associated glomerulonephritis. Clin Nephrol 53：242－252, 2000
8) Ishida-Okawara A, Oharaseki T, Takahashi K, et al：Contribution of myeloperoxidase to coronary artery vasculitis associated with MPO-ANCA production. Inflammation 25：381－387, 2001
9) 鈴木和男：血管炎発症機構の解析研究-活性化好中球の関与. 医学のあゆみ 206：133－139, 2003
10) 鈴木和男：ANCA関連血管炎の発症機序-活性化好中球の関与. リウマチ科 29：228－236, 2003
11) Murata H, Iijima H, Naoe S, et al：The pathogenesis of experimental arteritis induced by Candida alkali-extract in mice. Jpn J Exp Med 57：305－313, 1987
12) Kinjoh K, Kyogoku M, Good RA：Genetic selection for crescent formation yields mouse strain with rapidly progressive glomerulonephritis and small vessel vasculitis. Proc Natl Acad Sci USA 90：3413－3417, 1993
13) Cherry Engelman RW, Wang BY, Kinjoh K, et al：Calorie restriction delays the crescentic glomerulonephritis of SCG/Kj mice. Proc Soc Exp Biol Med 218：218－222, 1998
14) Ishida-Okawara A, Ito Ihara T, Muso E, et al：Neutrophil contribution to the crescentic glomerulonephritis in SCG/kj mice. Nephrol Dial Transplant (in press)
15) Jayne DR, Chapel H, Adu D, et al：Intravenous immunoglobulin for ANCA-associated systemic vasculitis with persistent disease activity. QJM 93：433－439, 2000
16) Jayne DR：Update on the European Vasculitis Study Group trials. Curr Opin Rheumatol 13：48－55 (Review), 2001
17) Ito-Ihara T, Nogaki F, Ono T, et al：Intravenous immunoglobulin (IVIG) treatment of MPO-ANCA-related microscopic polyangiitis. Cleveland Clin J Med Suppl 69：SII－188, 2002

Available online at www.sciencedirect.com

SCIENCE DIRECT

Gene 334 (2004) 157–165

GENE
AN INTERNATIONAL JOURNAL ON GENES AND GENOMES

www.elsevier.com/locate/gene

A vitellogenin chain containing a superoxide dismutase-like domain is the major component of yolk proteins in cladoceran crustacean *Daphnia magna*☆

Yasuhiko Kato[1], Shin-ichi Tokishita[1], Toshihiro Ohta, Hideo Yamagata*

Laboratory of Environmental and Molecular Biology, Environmental Science Division, School of Life Science, Tokyo University of Pharmacy and Life Science, 1432-1 Horinouchi, Hachioji, Tokyo 192-0392, Japan

Received 8 January 2004; received in revised form 8 March 2004; accepted 29 March 2004
Available online 6 May 2004
Received by T. Gojobori

Abstract

A cDNA encoding vitellogenin (VTG), a precursor of a major yolk protein, vitellin (VTN), was isolated from cladoceran crustacean *Daphnia magna*. The deduced amino acid sequence of DmagVTG1, the polypeptide encoded by the cDNA, contained a possible signal peptide sequence of 16 amino acid (aa) residues. The possible mature form of DmagVTG1 consists of 1985 aa residues with a calculated molecular mass of 223,070 Da. The large lipid transfer (LLT) module and a part of the von Willebrand factor D (VWD) module found in the aa sequences of VTGs of many other organisms are well conserved in DmagVTG1. Phylogenetic analysis suggested that the LLT module of DmagVTG1 is more closely related to those of insect VTGs than those of decapodan crustaceans. A unique feature of DmagVTG1 is that it has a superoxide dismutase (SOD)-like domain at its NH_2-terminus. Antisera against the SOD-like domain, the NH_2-terminal part of the VTG domain and the COOH-terminal part of the VTG domain, respectively, were prepared and used for analysis of *D. magna* yolk proteins. Six species (I to VI) of major protein complexes were found in *D. magna* parthenogenetic eggs isolated immediately after ovulation. Complexes IV and V were the most abundant. DmagVTG1 was a component of Complexes III, IV and V, and the most abundant polypeptide in *D. magna* eggs. The protein complexes underwent gradual proteolysis during development. One of the primary sites of cleavage was between the two successive Arg residues located at the 1454th and 1455th positions of DmagVTG1.

Keywords: cDNA; Water flea; Vitellogenesis; Parthenogenetic egg; Endocrine disrupters; Proteolysis

1. Introduction

Vitellogenin (VTG), a major lipoprotein in many oviparous animals, is a precursor of major yolk protein vitellin (VTN). It has been shown that VTG is secreted by the liver in vertebrates, the intestine in nematodes and the fat body in insects, and then taken up by developing oocytes. During these processes, VTG and VTN are modified through cleavage, glycosylation, lipidation and phosphorylation (reviewed in Raikhel and Dhadialla, 1992; Sappington and Raikhel, 1998). They often form oligomeric complexes in their native states. Their monomers consist of one to four subunits. They serve as storage proteins providing amino acids, carbohydrates, lipids and phosphates to the developing embryo (Byrne et al., 1989). They also serve as trace mineral-transporting proteins (Falchuk and Montorzi, 2001). Accumulation of VTG or VTN in oocytes is one of the key events in the process of ovarian maturation. This physiological process, known as vitellogenesis, is usually

Abbreviations: VTG, vitellogenin; VTN, vitellin; cDNA, DNA complementary to RNA; SDS, sodium dodecyl sulfate; PAGE, polyacrylamide gel electrophoresis; PCR, polymerase chain reaction; SOD, superoxide dismutase; ORF, open reading frame; bp, base pair(s); aa, amino acid(s); kb, kilobase pair(s); kD, kilodalton(s); LLT, large lipid transfer; VWD, von Willebrand factor D; MTP, large subunit of microsomal triglyceride transfer protein.

☆ The nucleotide sequence reported in this paper has been submitted to the DDBJ/EMBL/GenBank Data Banks under accession number AB114859.

* Corresponding author. Tel.: +81-426-76-7053; fax: +81-426-76-7081.
E-mail address: yamagata@ls.toyaku.ac.jp (H. Yamagata).

[1] Equally contributed to this work.

0378-1119/$ - see front matter © 2004 Elsevier B.V. All rights reserved.
doi:10.1016/j.gene.2004.03.030

under the control of several hormones and has been extensively studied as a model system for the hormonal control of genes at the molecular level. Its regulatory mechanisms have been well defined in oviparous vertebrates and insects (Arukwe and Goksoyr, 2003). In crustaceans, much less is known concerning its regulation and associated reproductive function, although many species are important targets of fishery and aquaculture development.

Several anthropogenic chemicals not specifically designed to possess hormonal activity, such as some pesticides and plasticizers, exhibit estrogen-like activities in vertebrates. This is because these agents are able to bind to the estrogen receptor (McLachlan and Arnold, 1996). Abnormal production of VTG by male fish after exposure to estrogenic xenobiotics is well documented (Arukwe and Goksoyr, 2003). Elevation of VTG in male madaka causes significant reproductive impairment (Gronen et al., 1999). Thus, VTG and VTN are also important from the viewpoint of their use as biomarkers for the study of potential endocrine disrupters. Because of the role of cladocerans (water fleas) such as *Daphnia* as an important link in the food webs of freshwater ecosystems, and because they are the oldest and most widely used test organisms in aquatic toxicology, whether or not hormonally active xenobiotics have adverse effects upon their endocrine processes is of special concern.

Although VTG genes and cDNAs have been investigated in a wide range of animals, both in vertebrates and invertebrates, no cladoceran VTG gene or cDNA has been reported yet. In this work, we isolated a *Daphnia magna* VTG cDNA and characterized its product. Interestingly, the polypeptide encoded by the cDNA had a superoxide dismutase (SOD)-like domain at its NH_2-terminus.

2. Materials and methods

2.1. cDNA cloning and DNA sequencing

A 1-kb cDNA fragment encoding a polypeptide whose amino acid sequence (from the 1768th to 2001st amino acids, Fig. 1) shows considerable homology to those of the COOH-terminal regions of known VTGs was found fortuitously among the fragments that gave false positive signals on differential display analysis of *D. magna* transcripts. This cDNA fragment was labeled and used for screening of the *D. magna* cDNA library constructed previously (Tokishita et al., 1997), with the aid of a DIG DNA Labeling Kit and a DIG Nucleic Acid Detection Kit (Roche). One positive clone, λ-*DmagVtg1*, was isolated and subsequently analyzed. DNA sequencing was performed using an Applied Biosystems *Taq* DyeDeoxy Terminator Sequencing Kit and an ABI 377 automated sequencer.

2.2. Expression of cDNA fragments in Escherichia coli and preparation of antisera against the products

cDNA fragments encoding the SOD-like domain (SOD′, amino acids 26 to 170), the NH_2-terminal part (VTG/N, amino acids 590 to 881) of the VTG domain and the COOH-terminal part (VTG/C, amino acids 1691 to 1990) of the VTG domain, respectively (Fig. 1), were amplified by polymerase chain reaction (PCR), and then expressed in the *E. coli* pET System (Novagen). The SOD-like domain was produced in a soluble form as a protein fused with thioredoxin using the pET-32b expression vector. The SOD-like domain was cleaved off from the fused protein by enterokinase treatment, separated by sodium dodecyl sulfate (SDS)-polyacrylamide gel electrophoresis (PAGE), and then recovered from the gel by electrophoresis. VTG/N and VTG/C were directly produced using the pET-19b expression vector, and then separated and recovered as above. The recovered polypeptides were used for the immunization of rats.

2.3. Extraction of proteins from D. magna eggs at various developmental stages

D. magna Straus obtained from the National Institute for Environmental Studies, Japan was used. The reared animals were inspected individually for maturation of the ovaries. Animals with mature ovaries were selected and watched further. When ovulation occurred, the animal was transferred to a separate flask (time 0). Eggs (or embryos) were isolated from the brood chamber at various stages of development (0–48 h) and stored at −80 °C. To extract total proteins, the stored eggs were suspended in 5 μl/egg of an extraction solution comprising 25 mM Tris–HCl (pH 8.8), 0.05% 3-[(3-cholamidopropyl)dimethylammonio]-1-propanesulfonate (CHAPS, Wako, Japan), Protease Inhibitor Cocktail (Roche, Complete, Mini, EDTA-free, 1 tablet in 10 ml) and 3 ng/ml of Pepstatin A (Wako), and homogenized on ice with a plastic pestle, and then a supernatant was obtained by centrifugation at 20,000 × *g* for 5 min at 4 °C.

2.4. Gel electrophoresis and determination of NH_2-terminal amino acid sequence

SDS-PAGE was performed with 6% separating and 4.5% stacking gels as described (Laemmli, 1970). 5.5% separating and 4.5% stacking gels were used for native PAGE, SDS and β-mercaptoethanol being omitted from the running buffer and sample solution. Western blot analysis was performed with the aid of an ECL plus Western Blotting Detection System (Amersham Biosciences). Two-dimensional gel electrophoresis and NH_2-terminal amino acid sequence determination were performed as described previously (Kimura et al., 1999; Kato et al., 2001). HRP-ConA

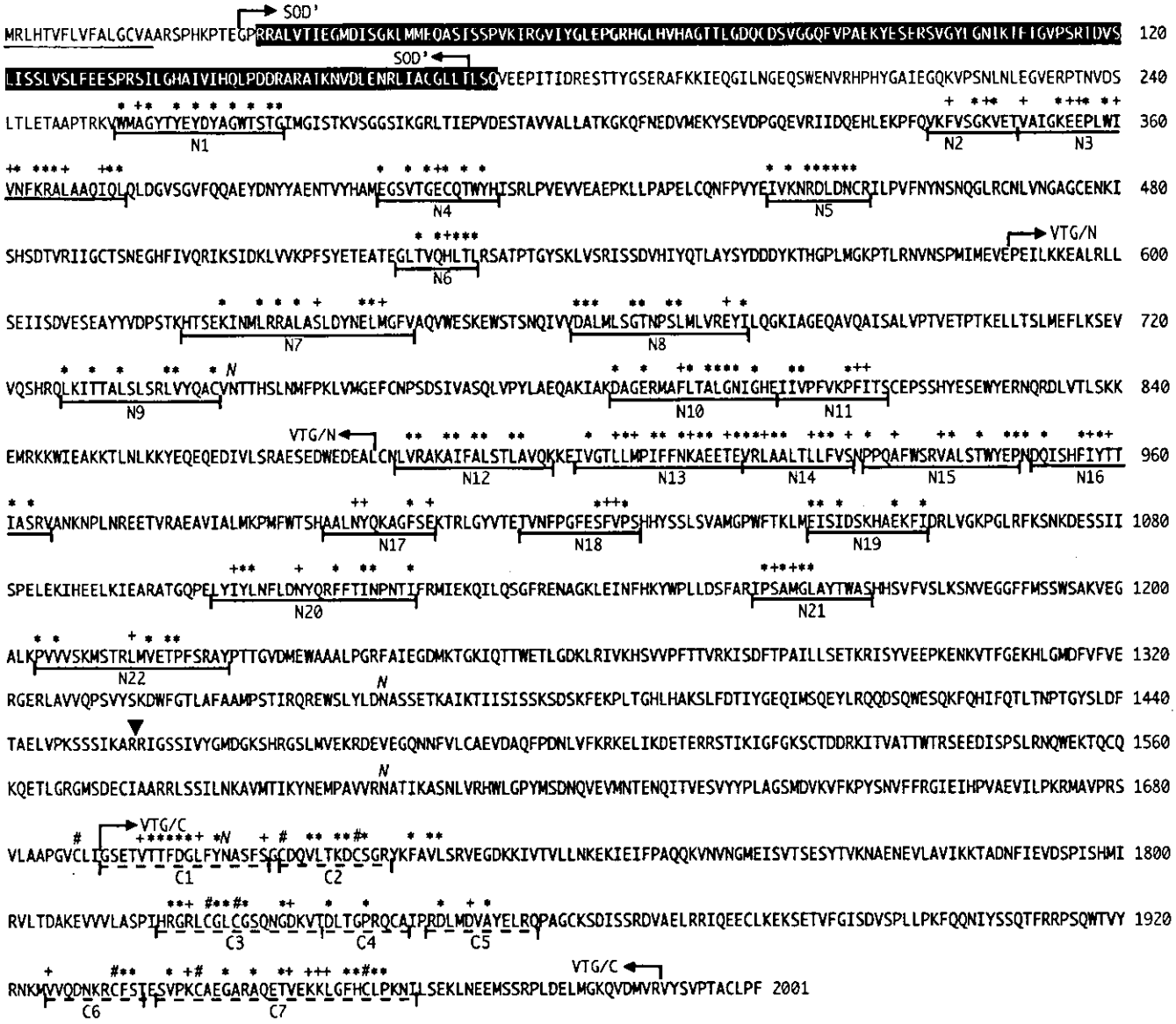

Fig. 1. The deduced amino acid sequence of the *D. magna* vitellogenin chain, DmagVTG1. The SOD-like and VTG domains are shadowed in black and gray, respectively. The sequence(s) constituting the possible signal peptide, LLT motifs (N1 to N22) and VWD motifs (C1 to C7) are underlined with a thin line, thick lines, and thick broken lines, respectively. Residues that match the multilevel consensus sequence (Babin et al., 1999) are indicated by asterisks. Plus signs indicate that similar amino acid residues are conserved in the known LLT and VWD motifs. Cys residues highly conserved in the known VWD motifs are denoted by sharps. An arrowhead indicates the primary cleavage site determined in this work. The positions of the polypeptides used as antigens are shown at the top of the sequence (SOD', VTG/N and VTG/C). Potential N-linked glycosylation sites are denoted by *N*.

(Seikagaku Kogyo, Japan) was used for glycoprotein-specific staining.

3. Results

3.1. Characterization of a cDNA encoding D. magna vitellogenin

A clone named λ-*DmagVtg1* was isolated as described in Section 2.1. The nucleotide sequence of the cDNA inserted in λ-*DmagVtg1* comprises 6335 bp including a 28-bp 5′-untranslated region (UTR), a 6006-bp open reading frame (ORF) starting at the first Met codon, ATG, and ending with a stop codon, TAA, and a 282-bp 3′-UTR (excluding a 19-bp poly-A tail). The sequence, AATAAATAAA, located 19-bp upstream from the poly-A sequence was considered to comprise overlapped poly-adenylation signals (not shown). The predicted amino acid sequence of the product of the ORF, DmagVTG1, is shown in Fig. 1.

The amino acid sequence from the first Met to the 16th residue (underlined in Fig. 1) shows the characteristic features of signal peptides of eukaryotic secretory proteins,

including the presence of a positively charged residue near the NH_2-terminus (Arg2), a hydrophobic stretch in the central region (from Val6 to Leu12), a small residue at the −1 position (Ala16), and the absence of an aromatic, charged or large-polar residue (Asn or Gln) at the −3 position (Von Heijne, 1986). DmagVTG1 is most probably synthesized as a secretory precursor with a signal peptide of 16 amino acid residues. The deduced mature product consists of 1985 amino acid residues with a molecular mass of 223,070 Da. The four Asn residues at the 745th, 1361st, 1601st and 1704th positions constitute potential N-linked glycosylation sites (NXT/S).

3.2. The LLT and VWD modules

Twenty-two ungapped conserved sequence motifs (N1 to N22) have been identified in the most conserved NH_2-terminal parts of large lipoproteins, such as VTG, apolipo-

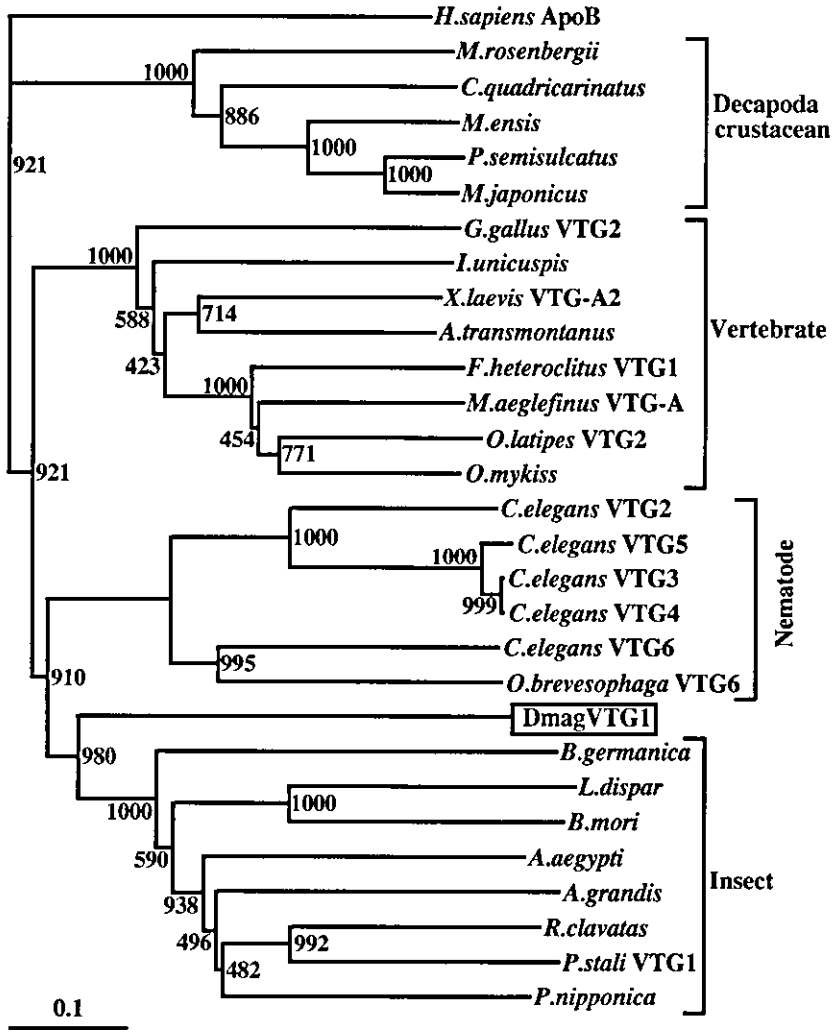

Fig. 2. A phylogenetic tree of the amino acid sequences of various LLT modules. The LLT modules used in this analysis and their accession numbers in the genbank/EMBL/DDBJ or SWISS-PROT databases are: DmagVTG1 (AB114859, this work); VTGs of insects, *Blattella germanica* (German cockroach, CAA06379), *Lymantria dispar* (gypsy moth, AAC02818), *Bombyx mori* (silkworm, D13160), *Aedes aegypti* (yellow fever mosquito, U02548), *Anthonomus grandis* (boll weevil, M72980), *Riptortus clavatus* (bean bug, U97277), *Plautia stali* VTG1 (brown winged green bug, BAA88075) and *Pimpla nipponica* (parasitoid wasp, AF026789); VTGs of decapoda crustaceans, *Macrobranchium rosenbergii* (giant freshwater prawn, AB056458), *Cherax quadricarinatus* (crayfish, AF306784), *Metapenaeus ensis* (white shrimp, AF548364), *Penaeus semisulcatus* (green tiger shrimp, AY051318) and *Marsupenaeus japonicus* (kuruma prawn, AB033719); VTGs of vertebrates, *Gallus gallus* VTG2 (chicken, M18060), *Ichthyomyzon unicuspis* (silver lamprey, M88749), *Xenopus laevis* VTG-A2 (African clawed frog, M18061), *Acipenser transmontanus* (white sturgeon, U00455), *Fundulus heteroclitus* VTG1 (mummichog, U07055), *Melanogrammus aeglefinus* VTG-A (haddock, AAK15158), *Oryzias latipes* VTG2 (Japanese medaka, BAB79591) and *Oncorhynchus mykiss* (trout, X92804); VTGs of nematodes, *Caenorhabditis elegans* VTG2 (X56212), VTG3 (AAK09075), VTG4 (P18947), VTG5 (X03044) and VTG6 (X56213), and *Oscheius brevesophaga* VTG6 (Q94637) and *Homo sapiens* ApoB (apolipoprotein B, P04114). The ApoB sequence was used as an outer group sequence. The tree was constructed using the program CLUSTAL X37 (Thompson et al., 1997). The default parameters were used. Bootstrap values for 1000 replicate analyses are shown at branching points. The standard bar at the bottom shows the branch length corresponding to the mean number of differences (0.1) per residue along each branch.

protein B (ApoB) and large subunit of microsomal triglyceride transfer protein (MTP), from invertebrates and vertebrates (Babin et al., 1999; Shoulders et al., 1994). These multiple signature motifs, present in a fixed order, are located in the NH_2-terminal β-barrel-like domain (N1 to N6), the α-helical domain (N7 to N16), the linking segment (N17 to N20) and the β-pleated sheet domain (N21 to N22) in the VT1 subunit of lamprey VTG (Banaszak et al., 1991). A protein module composed of these motifs is named large lipid transfer (LLT; Hegyi and Bork, 1997). All 22 motifs were found in the amino acid sequence of DmagVTG1 (Fig. 1). Many amino acid residues are conserved in these motifs, including those indicated by asterisks in Fig. 1 that match the proposed multilevel consensus sequence (Babin et al., 1999). By analogy with the structure of lamprey VTG, Cys408 in N4 and Cys452 in N5 should form a disulfide linkage, and stabilize the NH_2-terminal β-barrel-like structure. Arg921 in N14 and Glu948 in N15 should form a salt bridge stabilizing the local fold of the α-helical domain (Mann et al., 1999). Lys445 in N5 is important for interaction with the VTG receptor (Li et al., 2002). N11 and N12, separated by a short sequence (7 or 8 amino acid residues) in the VTGs of other organisms, are separated by a sequence comprising 67 amino acid residues, many of which are charged, in DmagVTG1.

Seven conserved ungapped sequence motifs (C1 to C7) common to the COOH-terminal parts of VTG molecules were also found in the COOH-terminal part of DmagVTG1 (Fig. 1). These motifs are part of the VWD module found in the von Willebrand factor (VWD; Bonthorn et al., 1986) and other proteins including ApoB (Babin et al., 1999). Several highly conserved Cys residues are present in this region. In particular, a CGLCG motif reminiscent of the active sites of proteins catalyzing disulfide bond formation is located in the middle of this module. These residues have been considered to play a role in the formation of disulfide-linked multimers (Peretz-Vilar and Hill, 1998). Polyserine domains found in vertebrate and some insect VTGs (Chen et al., 1997) are missing in DmagVTG1.

3.3. Phylogenetic analysis of DmagVTG1

Phylogenetic trees were constructed from the conserved amino acid sequences of the LLT modules of known VTGs and DmagVTG1. The LLT modules of the known VTGs are grouped into separate clusters: insect, nematode, vertebrate, and decapodan crustacean (Fig. 2). The LLT module of cladoceran crustacean VTG, DmagVTG1, did not belong to the decapodan crustacean cluster but to the insect cluster.

3.4. The SOD-like domain at the NH_2-terminus of DmagVTG1

The most striking feature of DmagVTG1 is that the amino acid sequence of its NH_2-terminal part (Arg28 to Gln173; Fig. 1, shadowed in black) shows significant homology to that of Cu/Zn-type superoxide dismutase, which contains Cu(II) and Zn(II) in its active site (Cu/ZnSOD; Bordo et al., 1994). The amino acid sequence of the SOD-like domain of DmagVTG1 is aligned with those

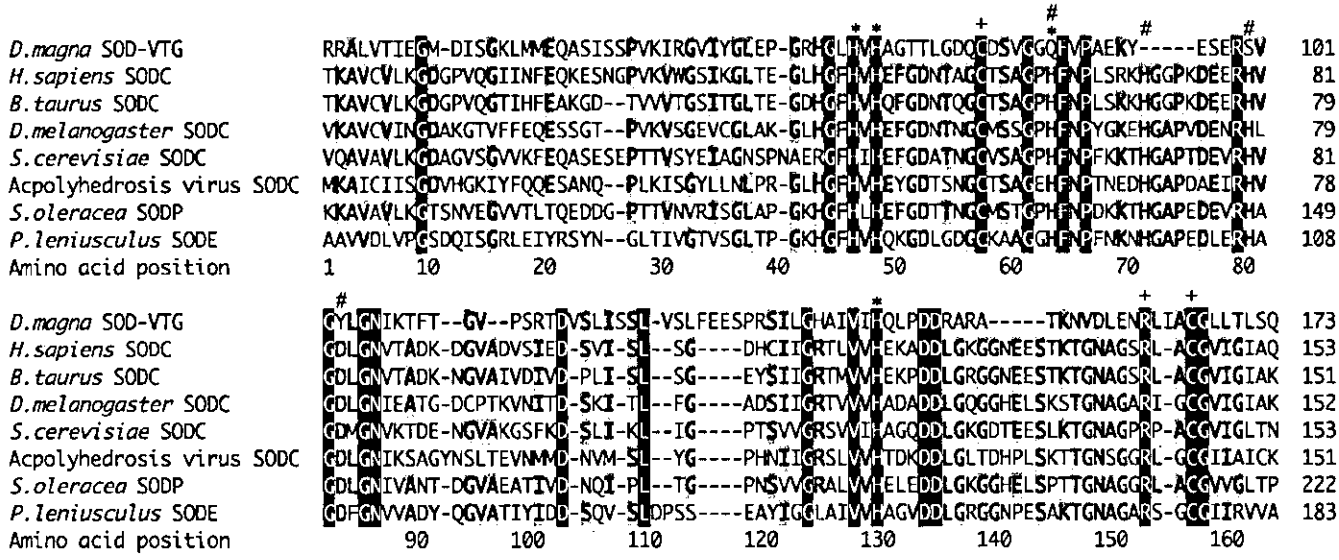

Fig. 3. Amino acid sequence alignment of the SOD-like domain and various Cu/Zn-SODs. The sequences used in this alignment and their accession numbers in the genbank/EMBL/DDBJ or SWISS-PROT database are: *D. magna* SOD-VTG (DmagVTG1, this work), *H. sapiens* SOD-C (cytosol type) (X02317), *B. taurus* SOD-C (bovine, M81129), *D. melanogaster* SOD-C (fruit fly, M24421), *S. cerevisiae* SOD-C (yeast, J03279), *Autographa californica* polyhedrosis virus SOD-C (baculovirus, M68862), *S. oleracea* SOD-P (chloroplast type) (spinach, D10244) and *P. leniusculus* extracellular SOD-E (extracellular type) (crayfish, AF122900). Gaps inserted to maximize the matching are denoted by hyphens. The amino acid position numbers in this alignment are shown at the bottom. The amino acid number of the last residue in each SOD sequence is shown to the right of the sequence. Residues conserved in all SOD sequences are shadowed in black. Other highly conserved residues are shadowed in gray. For other symbols, see Section 3.4.

of Cu/ZnSOD from various organisms in Fig. 3. More than 30% of the residues in the *Daphnia* sequence are identical with those of known Cu/ZnSODs at corresponding positions. For example, the *Daphnia* sequence shows 35.6%, 32.2% and 32.2% identity with the sequences of human and fruit fly cytosol SOD (SOD-C), and crayfish extracellular SOD (SOD-E), respectively. Among the highly conserved residues, the two Cys and one Arg residue at amino acid positions 57, 156 and 152 in Fig. 3 (Cys82, Cys166 and Arg162 in the *D. magna* sequence, denoted by +) are important for maintenance of the structure and activity of SOD (Fisher et al., 1994). The four His residues at positions 46, 48, 63 and 129, indicated by asterisks, are involved in the binding of Cu(II). His at position 63 is also required for the binding of Zn(II). Besides this His, His at positions 71 and 80, and Asp at position 83, indicated by sharps, are required for the binding of Zn(II) (Bordo et al., 1994). All of these Zn-binding residues are substituted or deleted in the *D. magna* SOD-like domain. The sequence of 80 amino acid residues that links the SOD-like domain to the VTG domain did not exhibit any significant homology with known sequences.

3.5. DmagVTG1 is the most abundant polypeptide in D. magna eggs at initial stages of development

To determine whether or not *D. magna* eggs contain a VTG chain fused with the SOD-like domain, antisera against the SOD-like domain, the NH_2-terminal part of the VTG domain and the COOH-terminal part of the VTG domain (named anti-SOD', anti-VTG/N and anti-VTG/C, respectively) were prepared as described in Section 2.2. Proteins present in *D. magna* eggs at early stages (0–10 h) of development were subjected to SDS-PAGE followed by Western blot analysis. A predominant band corresponding to a molecular mass of 220 kDa was observed at initial stages (0–2 h) of development (Fig. 4A). The 220-kDa polypeptide should represent DmagVTG1, because it was recognized by anti-SOD', anti-VTG/N and anti-VTG/C (Fig. 4B,C and D).

While the amount of the 220-kDa polypeptide decreased continuously at early stages (0–10 h) of development (Fig. 4A), the amounts of polypeptides with apparent molecular masses of 155, 150 and 90 kDa increased during this period, as detected with anti-SOD' (Fig. 4B). Essentially the same pattern was observed when anti-VTG/N was used for detection (Fig. 4C). These polypeptides except for the 220-kDa one were not observed when anti-VTG/C was used for detection. Instead, polypeptides with molecular masses of 130, 70 and 65 kDa were predominantly observed (Fig. 4D). The NH_2-terminal amino acid sequences of the major polypeptides described above were analyzed after their separation with the aid of two-dimensional gel electrophoresis. The NH_2-terminal amino acid sequence of the 220-kDa polypeptide could not be determined by the phenyl-isothiocyanate method (Edman, 1956), suggesting

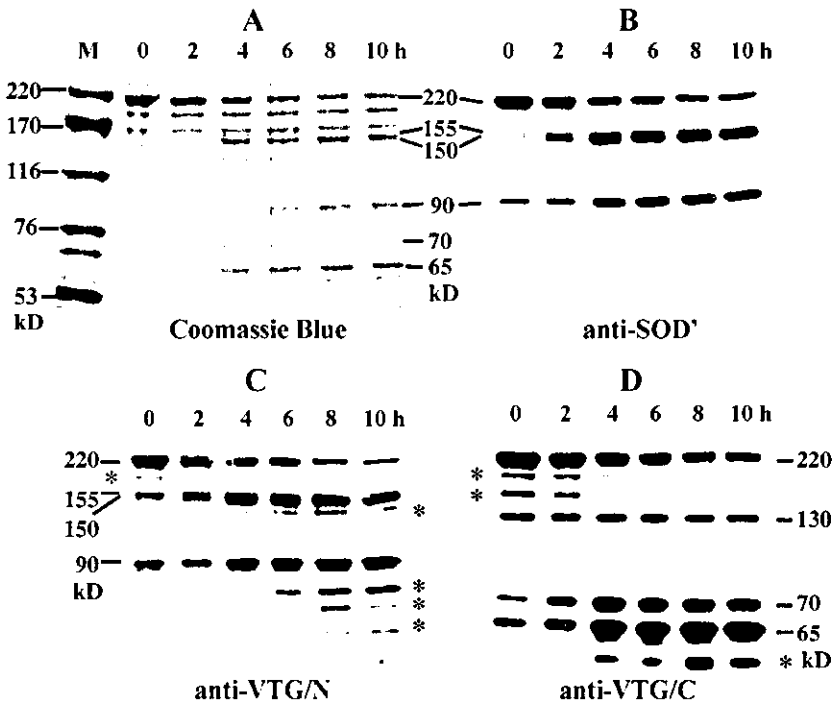

Fig. 4. SDS-PAGE and Western blot analysis of polypeptides present in *D. magna* eggs. Proteins extracted from *D. magna* eggs at early stages of development (0–10 h) were subjected to SDS-PAGE, and then staining with Coomassie Brilliant Blue (A) and Western blotting analysis, anti-SOD', anti-VTG/N and anti-VTG/C, respectively, being used for detection. Minor bands are indicated by asterisks. Extract corresponding to half of an egg was loaded in each well of the gel. M, molecular mass markers.

that the terminus is blocked. Only the NH_2-terminal amino acid sequence of the 65-kDa polypeptide has been determined so far. The determined sequence, Arg-Ile-Gly-Ser-Ser-Ile-Val-Tyr, is identical to that from the 1455th residue in the amino acid sequence of DmagVTG1 (Fig. 1), indicating that one of the primary cleavage sites of DmagVTG1 is between the two consecutive Arg residues located at the 1454th and 1455th positions.

3.6. DmagVTG1 is a component of major yolk protein complexes

Total protein fractions prepared from *D. magna* eggs (or embryos) at various stages of development were subjected to native PAGE. Six major protein bands corresponding to apparent molecular masses of higher than 500 kDa were found in the eggs at early stages of development (Fig. 5A, lanes 0 and 12 h). Since these bands were not observed on SDS-PAGE, they should represent oligomeric complexes of yolk proteins (designated as complexes I to VI according to their apparent molecular masses). Complexes IV and V were the most abundant. During the development of *D. magna* embryos (48 h), the amounts of these complexes gradually decreased, probably because of their proteolytic processing. All these protein complexes except for complex II were stained with Sudan Black B (Fig. 5B), indicating that they contain lipoproteins (De Vlaming et al., 1977). Concanavalin A-mediated staining (Kijimoto-Ochiai et al., 1985) showed that complexes III, IV, V and VI contain glycoproteins (Fig. 5C). Anti-SOD', anti-VTG/N and anti-VTG/C reacted to complexes III, IV and V (Fig. 5D,E and F), showing that these complexes contain DmagVTG1.

4. Discussion

The present results clearly demonstrate that DmagVTG1, a VTG chain with a Cu/ZnSOD-like domain at its NH_2-terminus, is the most abundant polypeptide constituting yolk protein complexes in *D. magna* eggs. Such a fusion VTG has never been found in other organisms. Cu/ZnSOD is considered to play a crucial role in the protection of oocytes and embryonic cells against oxygen toxicity in other organisms. It accumulates progressively during oocyte growth, in parallel with the accumulation of many other components such as yolk, mitochondria, ribosomes and mRNAs. Its level is maintained during embryogenesis in spite of changes in oxygen consumption (Montesano et al., 1989). The SOD-like domain fused with VTG may play a role in immediate detoxification of superoxides resulting from VTG metabolism. Analysis of purified complexes IV and V showed that the SOD activity corresponding to one chain of DmagVTG1 was about 1% of that of bovine Cu/Zn SOD (not shown). This level of activity may be enough for an adequate total activity level, because there is plenty of DmagVTG1 in *D. magna* eggs. Another possibility is that DmagVTG1 does not play a significant role in the detoxification of superoxides. It may be important only as a transporter of Cu(II). Since the aa residues constituting the

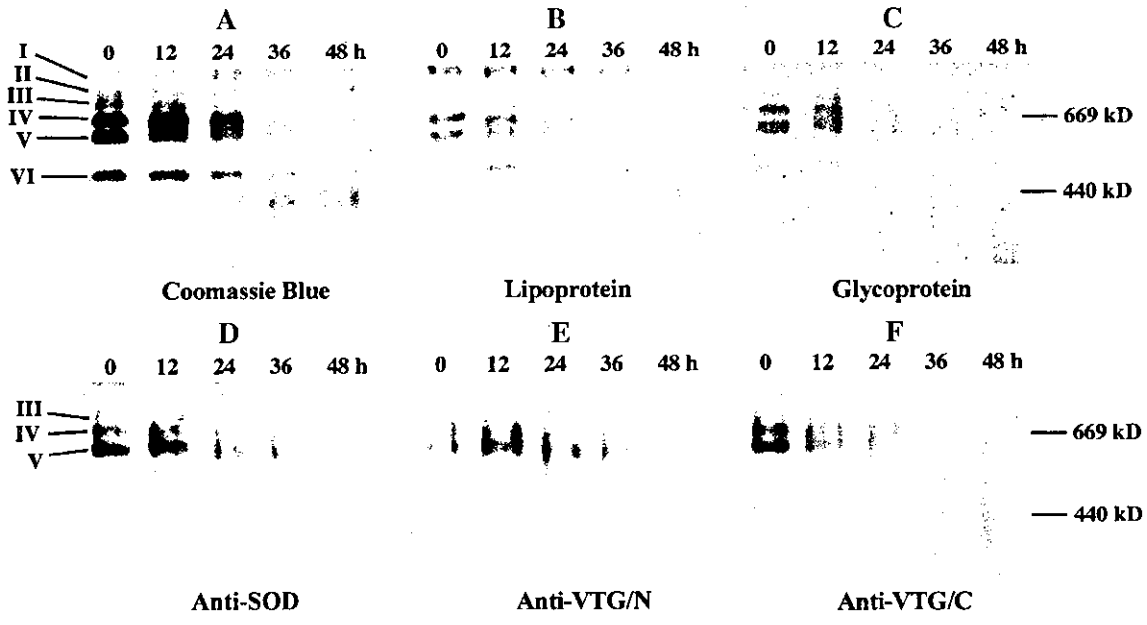

Fig. 5. Protein complexes with high molecular masses in *D. magna* eggs. Total protein fractions prepared from *D. magna* parthenogenetic eggs (or embryos) at various developmental stages (0–48 h) were subjected to native PAGE. Proteins were analyzed by staining with Coomassie Brilliant Blue (A), lipoprotein-specific staining with Sudan Black B (B), glycoprotein-specific staining mediated by concanavalin A (C) and Western blotting, antisera against the SOD-like domain (anti-SOD'), the NH_2-terminal part of the VTG domain (anti-VTG/N), and the COOH-terminal part of the VTG domain (anti-VTG/C), of DmagVTG1, respectively, being used for detection (D, E and F). Extract corresponding to one egg was loaded in each well of the gel.

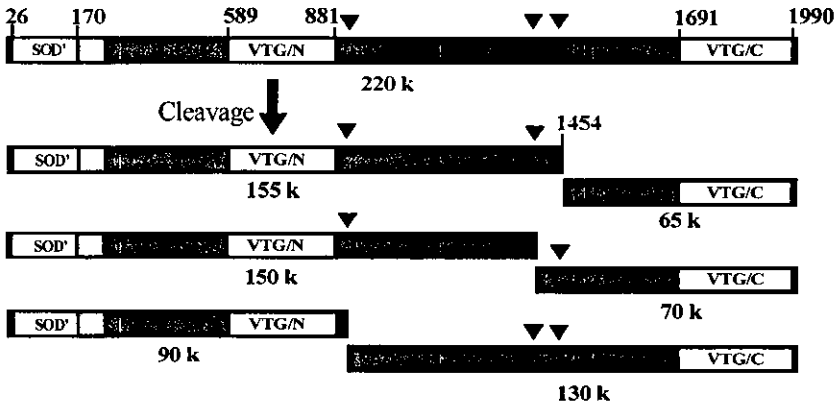

Fig. 6. Schematic representation of the primary cleavage sites in DmagVTG1. Arrowheads indicate the positions of the primary cleavage sites, and SOD', VTG/N and VTG/C, the positions of the polypeptides used as antigens.

binding site for Zn(II) are substituted or deleted, the SOD-like domain of DmagVTG1 probably does not contain Zn(II). The low SOD activity of DmagVTG1 may be ascribable to the absence of Zn(II). The metal content of the SOD-like domain has not been determined yet because of the difficulty in distinguishing the metals present in the SOD-like domain from those bound to the VTG domain.

Phylogenetic analysis of the LLT modules may suggest that DmagVTG1 is more closely related to insect VTGs than decapodan crustacean VTGs. It is not clear at present whether the LLT modules of DmagVTG1 and insect VTGs are closely related as to their divergence or their amino acid sequences resemble each other as a result of convergence. If the former possibility is the case, the close evolutionary relationship of cladocerans and insects, or horizontal transfer of the VTG gene between them is suggested.

Most VTG chains in other organisms are cleaved at some stage before the beginning of embryo development, for example, soon after their incorporation into oocytes in vertebrates (Byrne et al., 1989) or soon after their synthesis in the fat body in insects (Raikhel and Dhadialla, 1992). The resulting cleavage products usually constitute the subunit chains of VTN complexes. In the case of DmagVTG1, full-size chains constitute the major component of yolk protein complexes at initial stages of development. The results shown in Fig. 4 can be explained as follows; most DmagVTG1 chains (220 kDa) are primarily cleaved at either of three sites in the central region, giving rise to 90- and 130-kDa polypeptides, 150- and 70-kDa polypeptides, and 155- and 65-kDa polypeptides, respectively (Fig. 6). The minor bands indicated by asterisks in Fig. 4C and D suggest that cleavage at other sites than the above described three occurs at relatively low frequency. That one of the primary cleavage sites of DmagVTG1 is between two successive Arg residues suggests the involvement of enzymes similar to N-arginine dibasic convertase (Seidah and Prat, 2002).

Analysis of the structure of the gene for DmagVTG1, as well as analyses to examine whether *D. magna* eggs contain SOD species not fused with VTG and whether SOD-VTG fusion is commonly observed in other lower crustaceans such as *Moina macrocopa*, are in progress to elucidate the evolutionary and physiological implications of the fusion. The cDNA for and antisera against DmagVTG1 described here should be useful tools for investigating the effects of xenobiotics on the endocrine processes in cladocerans.

Acknowledgements

This work was partly supported by a Grant-in-Aid for Scientific Research from the Ministry of Education, Science, Sports and Culture of Japan (1260067).

References

Arukwe, A., Goksoyr, A., 2003. Eggshell and egg yolk proteins in fish: hepatic proteins for the next generation: oogenetic, population, and evolutionary implications of endocrine disruption. Comp. Hepatol. 2, 4–24.

Babin, P.J., Bogerd, J., Kooiman, F.P., Van Marrewijk, W.J.A., Van der Horst, D.J., 1999. Apolipophorin II/I, apolipoprotein B, vitellogenin, and microsomal triglyceride transfer protein genes are derived from a common ancestor. J. Mol. Evol. 49, 150–160.

Banaszak, L., Sharrock, W., Timmins, P., 1991. Structure and function of a lipoprotein: lipovitellin. Annu. Rev. Biophys. Biophys. Chem. 20, 221–246.

Bonthorn, D.T., Handin, R.I., Kaufman, R.J., Wasley, L.C., Orr, E.C., Mitsock, L.M., Ewenstein, B., Loscalzo, J., Ginsburg, D., Orkin, S.H., 1986. Structure of pre-pro-von Willebrand factor and its expression in heterologous cells. Nature 324, 270–273.

Bordo, D., Djinovic, K., Bolognesi, M., 1994. Conserved patterns in the Cu,Zn superoxide dismutase family. J. Mol. Evol. 238, 366–386.

Byrne, B.M., Gruber, M., Ab, G., 1989. The evolution of egg yolk proteins. Prog. Biophys. Mol. Biol. 53, 33–69.

Chen, J.S., Sappington, T.W., Raikhel, A.S., 1997. Extensive sequence conservation among insect, nematode, and vertebrate vitellogenins reveals ancient common ancestry. J. Mol. Evol. 44, 440–451.

De Vlaming, V.L., Vodicnik, M.J., Bauer, G., Marquette, T., Evans, D., 1977. Estradiol-17 beta effects on lipid and carbohydrate metabolism